ICSV14
Cairns • Australia
9-12 July, 2007

STATIC OUTPUT FEEDBACK CONTROL FOR NON-LINEAR FLUTTER AND LIMIT CYCLE OSCILLATION

Morteza Dardel[1] and Firooz Bakhtiari-Nejad[2]

[1]PhD Student, Mechanical Engineering, AmirKabir University of Technology
[2]Professor of Mechanical Engineering, AmirKabir University of Technology, Hafez Ave. Tehran, Iran
mdardel@gmail.com, baktiari@aut.ac.ir

Abstract
Non-linear flutter and limit cycle oscillations (LCOs) control of a non-linear wing are considered here. For this purpose, at first, a new formulation of static output feedback control is developed, and then an optimal solution for determining gains is presented. The optimal solution obtained from solving combined Lyapunov and Riccati equation. The designed controller applied for suppression of LCOs of low aspect ratio rectangular wings in low subsonic flow. This non-linear wing model has double bending in both chord-wise and span-wise directions (Von Karman plate theory). For aerodynamic modelling, a vortex lattice method is used. Results show, with this simple controller, we can effectively suppress limit cycle oscillation and extend flutter boundary.

1. INTRODUCTION

Many studies show that, aeroelastic systems are inherently nonlinear and behaviours such as jump phenomena, limit cycles, modal interactions, and various types of resonances occur in aeroelastic systems. Ref. [1] presents an excellent review of nonlinear aeroelasticity and related topics.

Many strategies applied to nonlinear flutter control of wings and airfoils, [2-3]. Here static output feedback (SOF) control method applied to flutter and limit cycle oscillation control of a nonlinear aero-elastic cantilevered wing in low subsonic flow. The structural model is a nonlinear plate model based on Von-Karman plate theory which can model both in-plane and transverse displacements. The structural nonlinearity is due to double bending in both chord-wise and span-wise directions. For aerodynamic modeling, a three dimensional vortex lattice aerodynamic model is used [4]. At first, we present a new solution method to solve this conceptually simple, but mathematically difficult control method and then applied it to a complex aeroelastic system.

2. STATIC OUTPUT FEEDBACK CONTROL

The static output feedback (SOF) problem is one of the most important open questions in linear control engineering. This control method applied by Patil and Hodges [5] to control of

nonlinear aeroelastic response of slender wing. Here, at first we present new static output feedback formulation, and then give an optimal solution based on this formulation.

Consider a linear time invariant system in the form of:

$$\dot{x}(t) = Ax(t) + Bu(t) \tag{1}$$

$$y(t) = Cx(t) \tag{2}$$

with control input as:

$$u(t) = -Ky(t) \tag{3}$$

We take $x(t) \in \Re^{m\times 1}$, control input $u(t) \in \Re^{n\times 1}$ and the output $y(k) \in \Re^{p\times 1}$. At first we divide states of system into two categories, measurable and unmeasurable, i.e.

$$x = \{x_1 \quad x_2\}^T \tag{4}$$

Here, we assume that $x_1 \in \Re^{p\times 1}$ are measurable, and $x_2 \in \Re^{(m-p)\times 1}$ are not measurable. Eq. (1) in terms of these variables can be written as:

$$\begin{aligned} \dot{x}_1(t) &= A_{11}x_1(t) + A_{12}x_2(t) + B_1u(t) \\ \dot{x}_2(t) &= A_{21}x_1(t) + A_{22}x_2(t) + B_2u(t) \end{aligned} \tag{5}$$

where A_{ij} and B_i are subsystems of A and B matrices, respectively. The output equation in terms of this variables can be written as,

$$y(t) = \begin{bmatrix} C_1 & 0 \end{bmatrix} \begin{Bmatrix} x_1(t) \\ x_2(t) \end{Bmatrix} = C_1x_1(t) \tag{6}$$

In which, $C_1 \in R^{p\times p}$ and invertible. In addition, Eq. (3) can be written as:

$$u(t) = -KC_1x_1(t) \tag{7}$$

With changing variables and combining Eq (7) with Eq. (5), dynamics of system can be written in compact form of

$$\dot{z}(t) = Gz(t) + Hu(t) \tag{8}$$

where,

$$z(k) = \begin{Bmatrix} y(k) \\ x_2(k) \end{Bmatrix}, \; G = \begin{bmatrix} C_1A_{11}{}_{p\times p}C_1^{-1} & C_1A_{12} \\ AC_1^{-1} & A_{22} \end{bmatrix}, \; H = \begin{bmatrix} C_1B_1 \\ B_2 \end{bmatrix}, \quad K' = \begin{bmatrix} K & 0 \end{bmatrix} \tag{9}$$

And

$$u(k) = -K'z(k) \tag{10}$$

2.1 POLE PLACEMENT TECHNIQUE FOR DETERMINING GAIN K

As usual in modern control method, one method for determining K is via pole placement technique. For this purpose, we introduce transformation $T \in R^{m\times m}$, which transform original system into canonical controllable form. If we apply this transformation to Eq. (8), the gains K can be determined from below equation (required manipulations are deleted):

$$KT_1 = [\alpha_m - a_m \quad \alpha_{m-1} - a_{m-1} \quad \cdots \quad \alpha_2 - a_2 \quad \alpha_1 - a_1] \tag{11}$$

Where $T_1 \in R^{\mathrm{p\times m}}$ is part of transformation matrix $T = \begin{bmatrix} \mathrm{T}_1 & \mathrm{T}_2 \end{bmatrix}^T$. a_i and α_i are coefficients of open loop and closed loop characteristic equations, respectively.Since, T_1 is not a square matrix, we cannot solve Equation (11). If we chance to find inverse of non-square matrix of T_1, then we can assign poles of closed loop system in every desired location,

but this is not always possible, and we only must hope to find approximate solution for above equation. We can rewrite Eq. (11)

$$K\begin{bmatrix}T_{11} & T_{12}\end{bmatrix}=\begin{bmatrix}\alpha_m - a_m & \cdots & \alpha_{m\text{-}p} - a_{m\text{-}p} & \alpha_{m\text{-}p\text{-}1} - a_{m\text{-}p\text{-}1} & \cdots & \alpha_1 - a_1\end{bmatrix} \tag{12}$$

where $T_1 = \begin{bmatrix}\mathrm{T}_{11} & \mathrm{T}_{12}\end{bmatrix}$ and $\mathrm{T}_{11} \in R^{p\times p}$, $\mathrm{T}_{12} \in R^{p\times(m-p)}$. Equating different elements of Eq.(12) we have

$$KT_{11} = \begin{bmatrix}\alpha_m - a_m & \cdots & \alpha_{m\text{-}p} - a_{m\text{-}p}\end{bmatrix},\ KT_{12} = \begin{bmatrix}\alpha_{m\text{-}p\text{-}1} - a_{m\text{-}p\text{-}1} & \cdots & \alpha_1 - a_1\end{bmatrix} \tag{13}$$

From first equation of (13), we have

$$K = \begin{bmatrix}\alpha_m - a_m & \cdots & \alpha_{m\text{-}p} - a_{m\text{-}p}\end{bmatrix}T_{11}^{-1} \tag{14}$$

with substituting Equation (14) into second Equation (13), we have,

$$\begin{bmatrix}\alpha_{m\text{-}p\text{-}1} - a_{m\text{-}p\text{-}1} & \cdots & \alpha_1 - a_1\end{bmatrix} = \begin{bmatrix}\alpha_m - a_m & \cdots & \alpha_{m\text{-}p} - a_{m\text{-}p}\end{bmatrix}T_{11}^{-1}T_{12} \tag{15}$$

From Eq. (15), we conclude that, when full states measurement is not possible, we are not free in specifying all coefficient of closed loop characteristic equation and we can only change p coefficients. Since determining gain K from above procedure is not possible, we present optimal solution for this problem.

2.2 *OPTIMAL STATIC OUTPUT FEEDBACK SOLUTION*

Considering a cost function in the form of:

$$J = \int_{t_o}^{\infty}\left[z^T Q z + u^T R u\right]dt \tag{16}$$

Minimizing this cost function, results:

$$\dot{z}^T M z + z^T M \dot{z} = -z^T\left(Q + K'^T R K'\right)z \tag{17}$$

With replacing Eqs. (8) and (10) in (17), we have

$$\left[G - HK'\right]^T M + M\left[G - HK'\right] = -Q - K'^T R K' \tag{18}$$

At first dynamics of system partitioned as:

$$\mathrm{G} = \begin{bmatrix}\mathrm{G}_{11} & \mathrm{G}_{12}\\ \mathrm{G}_{21} & \mathrm{G}_{22}\end{bmatrix},\ \mathrm{H} = \begin{bmatrix}\mathrm{H}_1\\ \mathrm{H}_2\end{bmatrix} \tag{19}$$

where $\mathrm{G}_{11} \in R^{p\times p}$, $G_{12} \in R^{p\times(m-p)}$, $\mathrm{G}_{21} \in R^{(m-p)\times p}$, $\mathrm{G}_{22} \in R^{p\times p}$, $\mathrm{H}_1 \in R^{p\times n}$, $\mathrm{H}_2 \in R^{(m-p)\times n}$. With simplifying Eq. (18), we have,

$$\begin{aligned}\left(G_{11}^T - K^T H_1^T\right)M_{11} + \left(G_{21}^T - K^T H_2^T\right)M_{21} + M_{11}\left(G_{11} - H_1 K\right) + M_{12}\left(G_{21} - H_2 K\right)\\ + Q_{11} + K^T R K = 0\end{aligned} \tag{20}$$

$$G_{12}^T M_{11} + G_{22}^T M_{21} + M_{21}\left(G_{11} - H_1 K\right) + M_{22}\left(G_{21} - H_2 K\right) + Q_{21} = 0 \tag{21}$$

$$G_{12}^T M_{12} + G_{22}^T M_{22} + M_{21} G_{12} + M_{22} G_{22} + Q_{22} = 0 \tag{22}$$

Matrix K that minimizes J can be obtained by minimizing Eq. (20) with respect to K. With rewriting Eq. (20) as below,

$$G_{11}^T M_{11} + G_{21}^T M_{21} + M_{11} G_{11} + M_{12} G_{21} + Q_{11} - \left(M_{11} H_1 + M_{12} H_2\right)\left(H_1^T M_{11} + H_2^T M_{21}\right) + \left[R^{1/2} K - R^{-1/2}\left(H_1^T M_{11} + H_2^T M_{21}\right)\right]^T \left[R^{1/2} K - R^{-1/2}\left(H_1^T M_{11} + H_2^T M_{21}\right)\right] = 0 \quad (23)$$

Since, the last term is nonnegative, the minimum occurs when it is zero, or when,

$$\mathrm{K} = \mathrm{R}^{-1}\left(\mathrm{H}_1^{\mathrm{T}} \mathrm{M}_{11} + \mathrm{H}_2^{\mathrm{T}} \mathrm{M}_{21}\right) \quad (24)$$

Hence, Equations (20-22) are converted to,

$$G_{11}^T M_{11} + G_{21}^T M_{21} + M_{11} G_{11} + M_{12} G_{21} + Q_{11} - \left(M_{11} H_1 + M_{12} H_2\right) R^{-1}\left(H_1^T M_{11} + H_2^T M_{21}\right) = 0 \quad (25)$$

$$G_{12}^T M_{11} + G_{22}^T M_{21} + M_{21} G_{11} + M_{22} G_{21} + Q_{21} - \left(M_{21} H_1 + M_{22} H_2\right) R^{-1}\left(H_1^T M_{11} + H_2^T M_{21}\right) = 0 \quad (26)$$

$$G_{12}^T M_{12} + M_{21} G_{12} + G_{22}^T M_{22} + M_{22} G_{22} + Q_{22} = 0 \quad (27)$$

With solving Eqs. (25-27), matrix M can be obtained. We prepared a code for solving Eqs. (25-27), in which we transform these equations into algebraic nonlinear equations and then solve it. This code is applicable to case where all states are measurable. If it is requested, we can attach them to this paper.

3. AEROELASTIC MODELING

A schematic diagram of the wing-plate geometry with a three-dimensional vortex lattice model of the unsteady flow and piezoelectric patches showed in Fig. 1. The rectangular wing has span L, chord c, and thickness h. The aero-servo-elastic state space equations are derived based on assumed mode method and using Lagrange's equations based on the Von-Karman plate equations [15] using the total kinetic and elastic energies and the work done by applied aerodynamic and piezoelectric actuator forces on the plate. The modal functions used are axial and transverse natural modes of free-free and cantilevered rods and beams, respectively.

3.1 STRUCTURAL MODELING

The non-dimensional displacements equations are as follows [6].

$$\sum_k \sum_p C_{kp}^{ij} \bar{a}_{kp} + \sum_g \sum_f C_{gf}^{ij} \bar{b}_{gf} = C^{ij}, \qquad \sum_k \sum_p D_{kp}^{rs} \bar{a}_{kp} + \sum_g \sum_f D_{gf}^{rs} \bar{b}_{gf} = D^{rs} \quad (28\text{-}29)$$

$$\sum_m \sum_n \left[A_{mn}^{ij} \ddot{\bar{q}}_{mn} + B_{mn}^{ij} \bar{q}_{mn}\right] + F^{ij} + Q_{aero}^{ij} = Q_{piezo}^{ij} \quad (30)$$

where C_{kp}^{ij} and D_{gf}^{rs} are stretch stiffness matrices of wing in span-wise and chord-wise directions, and C_{gf}^{ij} and D_{kp}^{rs} are coupling stretch stiffness between displacements in span-wise and chord-wise directions and vise versa, respectively. Also C^{ij} and D^{rs} are non-linear forces which are quadratic polynomials of the plate transverse deflection [6]. $\bar{a}_{kp}$ and $\bar{b}_{gf}$ are generalized coordinates for span-wise and cord-wise displacements. And A_{mn}^{ij}, B_{mn}^{ij} and F_N^{ij} are mass, stiffness and nonlinear bending matrices. F_N^{ij} is a polynomial of order two and three

in terms transvers generalized coordinates $\bar{q}_{mn}$.

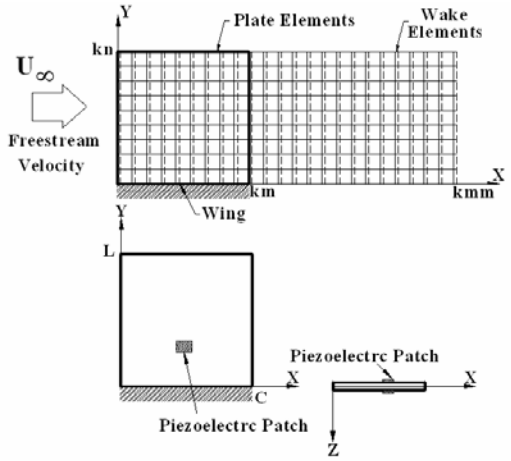

Fig. 1 Aero-servoelasrtic model of a cantilevered plate.

Q^{ij}_{aero} is the non-dimensional generalized force due to aerodynamic work [6]. Q^{ij}_{aero} is given by:

$$Q^{ij}_{aero} = \frac{\rho U^2 c^4}{6Dh}\int_0^1\int_0^1 \Delta\bar{p}\,\phi_i\varphi_j\,d\xi d\eta \qquad (31)$$

where ϕ_i and φ_j are assumed functions, which satisfy boundary conditions for transverse displacement. ρ and U are density and velocity of free stream, and D is bending stiffness of wing.

We assumed two similar piezoelectric patches with different sign applied voltages placed on the wing according to Fig. 1.

Hence, the net work down by piezoelectric actuators is from bending moment, and the stretching work will be diminished. The work down by piezoelectric patches will be given as [7]:

$$W_{piezo} = \frac{E_p h_p (h_p + h) d_{31}}{(1-\nu_p)} \iint_{A_p}\left[\frac{\partial^2 w}{\partial x^2} + \frac{\partial^2 w}{\partial y^2}\right] E_3\,dx\,dy \qquad (32)$$

where in Eq. (32), E_p, h_p, d_{31}, ν_p, and E_3 are, module of elasticity, thickness, dielectric constant, Poisson ratio, and applied electrical field of piezoelectric patches respectively. With assuming constant electric filed in poling direction of piezoelectric, the electric applied field E_3 relates to applied voltage V as $E_3 = V/h_p$. Hence generalized force due to piezoelectric actuator gives by:

$$Q^{ij}_{piezo} = 2Vd_{31}\frac{E_p}{E}\frac{1-\nu^2}{1-\nu_p}\left(\frac{c}{h}\right)^2\frac{h_p}{h}\left[1+\frac{h_p}{h}\right]\int_{\xi_{1p}}^{\xi_{2p}}\int_{\eta_{1p}}^{\eta_{2p}}\left[\phi_m''\varphi_n + \left(\frac{c}{L}\right)^2\phi_m\varphi_n''\right]d\xi d\eta \qquad (33)$$

where in Eq. (33), E, h, and ν are, module of elasticity, thickness, and Poisson ratio of wing, respectively.

3.2 *AERODYNAMICS MODELING*

An unsteady vortex lattice method is used to calculate the aerodynamic forces. The flow is assumed incompressible, inviscid, and irrotational. The plate and wake divided into a number of elements. In the wake and on the wing, all vortex elements have equal size Δx, in the stramwise direction. Vortex rings are place on the plate and in the wake at quarter chord of the elements. At the three-quarter cord of each plate element, a collocation point is placed for the downwash, i.e., the velocity induced by vortex rings are equal with downwash arising from unsteady motion of wing. As described in [6], the aerodynamic matrix equation can be expressed as

$$[A]\{\Gamma\}^{t+1} + [B]\{\Gamma\}^{t} = \{w\}^{t+1} \qquad (34)$$

where $[A]$ and $[B]$ are aerodynamic coefficient matrices, and $\{w\}^{t+1}$ is the non-

dimensional downwash at time step $t+1$ arising from the unsteady motion of wing.

3.3 *AEROSERVOELASTIC EQUATIONS*

With combining Eq.s (31), (32) and (30), we obtain coupled transverse and aerodynamic equations in matrix form (35), where the vector θ is the state of the plate, $\{\theta\} = \{\dot{q} \quad q\}^T$ and D_1 and D_2 are matrices describing the plate structural behavior , C_1 and C_2 are matrices describing the behaviours of distributed vortex elements on the plate itself. Eqs. (28-29) coupled with Eq. (35) represent complete aeroservoelastic state space equations.

$$\begin{bmatrix} A & -E \\ C_2 & D_2 \end{bmatrix} \begin{Bmatrix} \Gamma \\ \theta \end{Bmatrix}^{t+1} + \begin{bmatrix} B & 0 \\ C_1 & D_1 \end{bmatrix} \begin{Bmatrix} \Gamma \\ \theta \end{Bmatrix}^{t} = \begin{Bmatrix} 0 \\ -F_N + Q_{piezo} E_p \end{Bmatrix}^{t+1/2} \tag{35}$$

4. NUMERICAL RESULTS

The response of rectangular plate model, with and without control is considered. Here an aluminum alloy plate of constant thickness with aspect ratio of $AR \equiv L/c = 1$ is considered. The plate has stream-wise length $c = 0.3\,m$,thickness of $h = 0.001m$, and Poisson's ratio of $\upsilon = 0.3$. Plate and wake were modeled using 250 vortex rings, i.e., five elements in span-wise direction and fifty elements in stream-wise directions. For in-plane displacement eight modal numbers, i.e. four in streamwise and two in spanwise directions and for transverse displacements twenty modal numbers, i.e. ten in streamwise and two in spanwise directions are used. The vortex relaxation factor α assigned 0.992 .

Typical eigenvalues for the basic vortex lattice model obtained from Eq. (34) are shown in Figs. 2 and 3. Fig. 2 shows eigenvalues in terms of discrete–time multiplier z and Fig. 3. shows real and imaginary parts of the usual continuous–time eigenvalues λ . These results are in agreement with the results presented in [6].

When the non-linear force F_N and actuator force in Eq. (35), is set to zero, a linear aero-elastic model is obtained. Solving these equations for aero-elastic eigenvalues, determines the stability of the system. We increase speed from zero to arbitrary velocity and compute the dominate eigenvalues. When the real part of any eigenvalues becomes positive, the entire system becomes unstable. Fig.4 shows a typical representation of the eigenanalysis in the form of real eigenvalues as a function of the flow velocity. There are two intersections of $\mathrm{Re}(\lambda_i)$ with the velocity axis. One at $U_f = 42\,m/s$ for critical flutter velocity and the other is $U_d = 54.3\,m/s$ for divergent velocity. The results of this section are in complete agreement with results obtained by [18].

In order to investigate the nonlinear behaviour of limit cycle oscillation, complete aeroealstic Eqs. of (35) and (28-29), and without control input must be solved. A typical time histories of non-dimensional transverse displacements are shown in "Fig.s 4 and 5" . In "Fig. 4", the aerodynamics forces effectively damped the non-linear vibrations of the structure, but in "Fig. 5", aerodynamics and nonlinear structural forces are in equilibrium and non-linear system undergoes a limit cycle oscillation.

At the end, SOF controller designed for this system at velocity of $60\,m/s$ which is greater than linear flutter velocity With determining the optimal gain for resulting linear system, comparison of dominate poles of the closed loop and open loop poles are plotted in

Fig. 6. From this figure, we see that branches of open loop poles (o) move to right half of complex plane, but branches of closed loop poles $(+)$ move to the left half complex plan, and closed loop system becomes stable. Also real parts of eigenvalues versus velocity up to $60\,m/s$ is shown in Fig. 7.

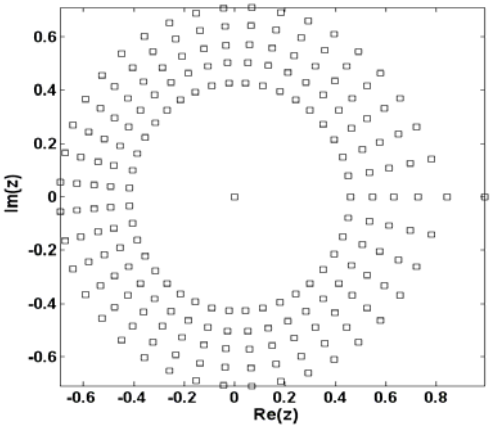

Fig:2. Discrete eigenvalues of aerodynamics model.

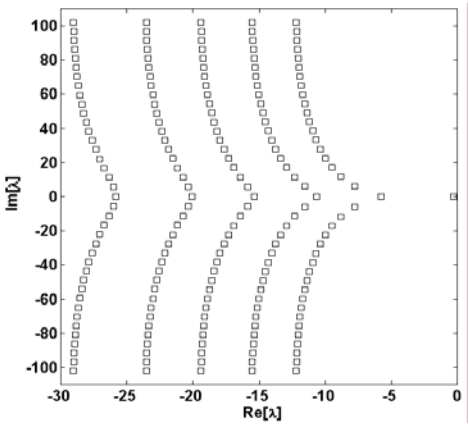

Fig 3: Eigenvalue solution of linear aeroelastic model.

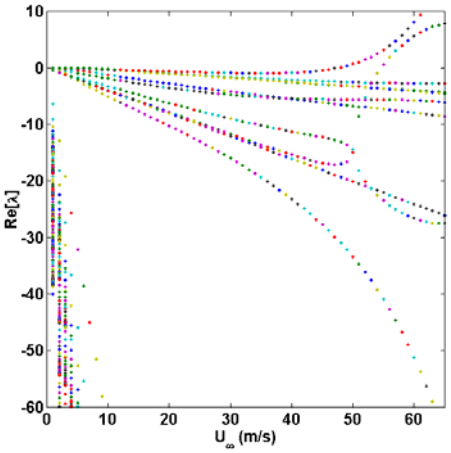

Fig 3: Eigenvalue solution of linear aeroelastic model.

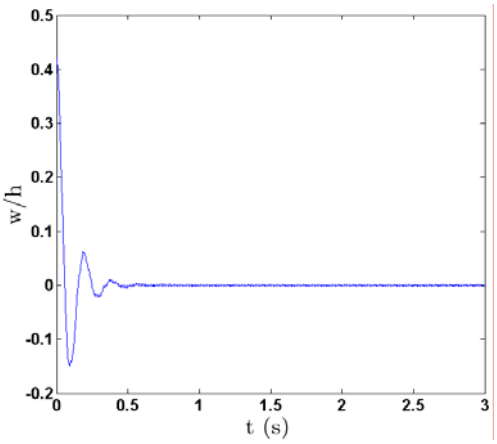

Fig 4: Transverse displacement at velocity of $40\,m/s$ (without control).

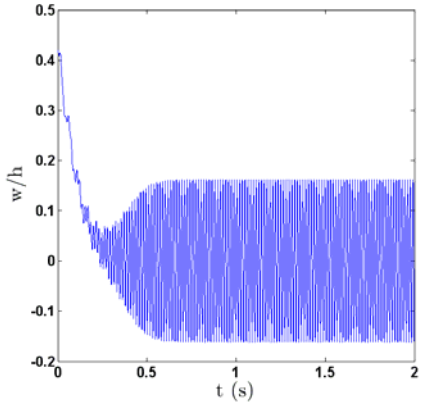

Fig 5: Transverse displacement at velocity of $60\,m/s$ (without control).

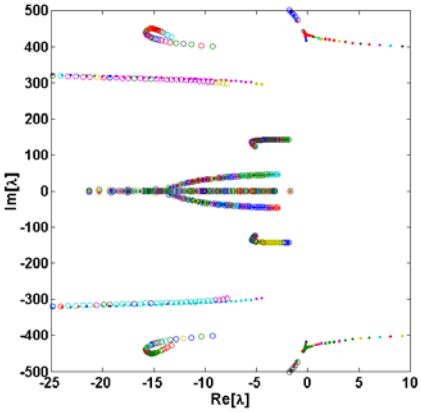

Fig. 6: Eigenvalue solutions of closed loop and open loop linear aeroelastic model with SOF

From this figure, we see that with increasing velocity, real parts of eigenvalues for linear open loop system becomes positive and system becomes unstable ($+$ symbol), but for closed

loop system, these poles remains negative (o symbol). Response of closed loop system at velocity greater than linear flutter velocity with SOF controller is shown in Fig. 8.

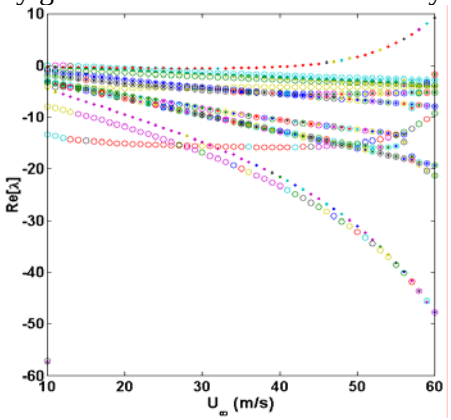

Fig:7. Real parts of eigenvalue of open and closed loops linear aeroelastic model.

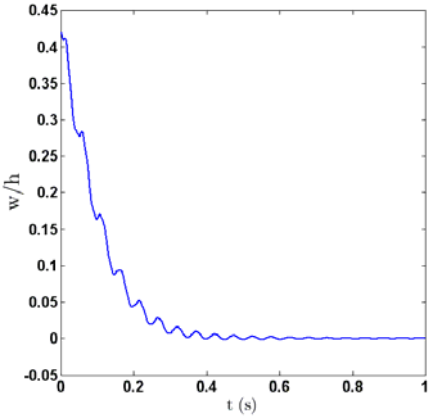

Fig 8: Transverse displacement at velocity of $60 m/s$ (with control).

5. CONCLUDING REMARKS

In the present work, limit cycle oscillation control of nonlinear aero-elastic wing with structural nonlinearity is considered. In this system limit cycle oscillation is due to counteractions of unstable poles of linear aero-elastic system and structural nonlinearity. The unstable poles tend to increase vibration amplitude, while structural nonlinearities tend to reduce this amplitude, and from these limit cycle results. Hence, if we stabilize these unstable poles, the whole system will be stable and limit cycle will be suppressed. For this purpose, a SOF controller is designed.Combination of above mentioned controller with linear part of aero-elastic system, push the unstable poles of the open loop system to left half of Laplace plane, and so the instability of linear part of the closed loop system is suppressed and limit cycle oscillation is diminished.

REFERENCES

[1] Dowell, E. H., Edwards, J., and Strganac, t. W., "Nonlinear Aeroelasticity", *Journal of Aircraft*, 40, 857-874,2003.

[2] Richard, R. E., Clark, R. L., "Delta Wing Flutter Control Using Spatially Optimized Transducers", *Intelligent Material Systems and Structures*, **14**, 677- 691,2003.

[3] Bhoir, N., and Singh, S. N., "Output Feedback Nonlinear Control of an Aeroelastic System with Unsteady Aerodynamics", *Aerospace Science and Technology,*8, 195-206, 2004.

[4] Hall, K.C., "Eigenanalysis of Unsteady Flows About Airfoils, Cascades, and Wings" , *AIAA Journal*,**32**, 2426-2423.

[5] Patil, M. J., and Hodges, D. H., "Output Feedback Control of the Nonlinear Aeroelastic Response of a Slender Wing," *Journal of Guidance, Control and Dynamics*, Vol. 25, No. 2, 2002, 302-308.

[6] Tang, D., Dowell, E.H., and Hall, K.C., "Limit Cycle Oscillation of a Cantilevered Wing in Low Subsonic Flow," *AIAA Journal*, 37, 3, 1999, 364-371.

[7] Hagood, N. W., Chung, W. H., and Folotow, A. V., "Modeling of Piezoelectric Actuator Dynamics For Active Structural Control," *Intelligent Material Systems and Structures*, Vol. **1**, 327-354,1990.